Numerical Investigation of Crossflow Separation on a Three-Caliber Tangent Ogive Cylinder

Leslie A. Yates* and Gary T. Chapman†
NASA Ames Research Center, Moffett Field, California

A parabolized Navier-Stokes code was used to calculate laminar crossflow separation on a simple body of revolution. Convergence lines were defined as lines on which skin-friction lines converge and were determined visually from the computed skin-friction patterns. These convergence lines were shown to be limit lines and not envelopes. Examination of crossflow cuts of stream tubes that encircled the body indicated that crossflow separation (defined by a fold in the stream tube) began after the onset of negative crossflow velocities but before a convergence line could be determined from the skin-friction patterns. There were no rapid changes or extrema in the pressure, skin-friction, vorticity, or flow-angle distributions that indicated where separation occurred. Instead, crossflow separation developed gradually and involved an extended region of the surface.

Introduction

CONSIDERABLE theoretical, experimental, and computational work has been undertaken in the last 30 years in an effort to understand the nature of three-dimensional flow separation. The topological approach used by Tobak and Peake[1,2] and the phenomenological approach used by Wang[3] have led to the definition of two classes of three-dimensional flow separation. The first class of separation, called global separation by Tobak and Peake and closed separation by Wang, has a saddle point associated with the flow separation, and the separation line is defined as one of the lines that pass through the saddle point (Fig. 1a). Chapman[4] has further subdivided this class of separation.

The second class of separation, called local separation by Tobak and Peake,[1,2] open separation by Wang,[3] and crossflow separation by Chapman,[4] develops gradually and results when the limiting streamlines squeeze together and fluid is forced away from the surface (Fig. 1b). There are no sudden changes when crossflow separation begins, and its onset is not easily defined. Furthermore, since no saddle points are associated with crossflow separation, the separation line cannot be defined as a line that passes through a saddle point. Instead, the separation line generally is defined to be a line on which skin-friction lines converge. In this text, this line will be called the convergence line.

The above definition does not provide a precise mathematical definition that will uniquely determine the convergence line. All lines that are converging on a line are converging upon each other, and any one of them can satisfy the above definition. However, it does appear from the visual inspection of skin-friction patterns (limiting streamline patterns) that there is one line on which all other lines converge. Unfortunately, since there is no precise mathematical definition of this line, it is not possible to determine whether this line is the continuation of a skin-friction line that begins at a node of attachment as suggested by Tobak and Peake[1,2] or if it is a line that begins anywhere on the body and does not follow a skin-friction line as suggested by Wang.[3] Also, it has proven difficult to determine whether this convergence line behaves as an envelope or as a limit line.

Even when a convergence line is observed, it is not possible to tell from the skin-friction pattern where crossflow separation occurs. Crossflow separation may begin before or after a convergence line is observed, and the existence of a visually observable convergence line alone does not guarantee separation.

A computational study has been performed in an effort to define the behavior of crossflow separation and the convergence line associated with it. A simple, axially symmetric body, a three-caliber tangent ogive cylinder, was chosen for these computations. By assuming supersonic flow, a space-marching code, the parabolized Navier-Stokes code, could be used, thus minimizing computational time and storage requirements. The static pressure, vorticity, and flow direction were studied in relation to the onset of crossflow separation.

Parabolized Navier-Stokes Code

The parabolized Navier-Stokes code used in this investigation is based on the Schiff-Steger algorithm[5] as further refined by Rai and Chaussee.[6] The finite-differencing scheme is second-order accurate in the marching direction and fourth-order accurate in the crossflow direction. It uses an implicit method to solve the parabolized Navier-Stokes equations in the computational plane (crossflow plane). The starting solutions were calculated using the parabolized Navier-Stokes code in the step-back mode. All computations were conducted for laminar flow conditions. Questions concerning the validity of turbulence models would have complicated the discussion of crossflow separation.

In the gridding scheme of Rai and Chaussee,[6] the grid points all lay on lines that radiated from the center of the body. These radial lines were equally spaced in the circumferential direction. This type of gridding scheme proved to be unsuitable for the study of crossflow separation. In the computations of crossflow separation, the skin-friction direction changed rapidly in the region near the convergence line. For some of these computations, the skin-friction direction changed by more than 20 deg when the circumferential angle changed by only 2.5 deg. Capturing these rapid changes with the unmodified gridding scheme would have required a very

Received Nov. 24, 1987; revision received March 30, 1988.

*Research Associate, National Research Council, NASA Ames Research Center. Member AIAA.

†Senior Staff Scientist, Thermosciences Division. Associate Fellow AIAA.

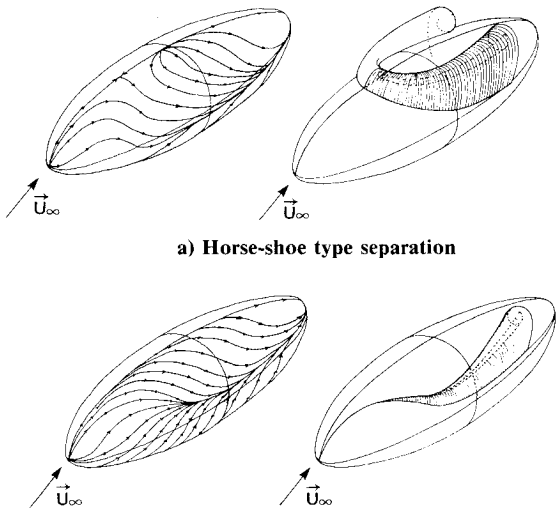

Fig. 1 Skin-friction patterns and surfaces of separation for two types of three-dimensional separation.

small spacing between radial lines and a large number of radial lines. However, since the skin-friction direction did not change rapidly except in the region near the convergence line, it was possible to resolve these rapid changes without using a large number of radial lines by clustering the radial lines toward the convergence line. This clustering was accomplished with a cubic function. Not only did this clustering improve the resolution of the solutions near the convergence line, it also improved the stability of the solutions.

The distance of the first grid point off the surface in the unmodified code[6] was given by one of two methods. In the first method, the physical distance of the first point off the surface was chosen to be constant. In the second method, the distance from the surface to the first point off the surface divided by the distance from the surface to the shock was chosen to be constant. In either case, the constant was independent of the circumferential angle and did not vary as the solution was marched. It could be changed only by stopping the marching procedure, inputting a new value for the constant, and restarting the solution. If a reasonable number of points were to be kept in the boundary layer as the solution was marched down the body, this constant had to be changed fairly often, about every caliber or so. Unfortunately, stopping the marching procedure, changing the locations of the first points off the surface, and restarting the solution introduced undesirably large oscillations in the axial pressure distributions and in the skin-friction orientation. Furthermore, this procedure did not take into account circumferential differences in the velocity field. In certain areas of the flow, there would not be a sufficient number of points in the boundary layer; in other areas of the flow, the velocity at the first grid point off the surface would be too small. This led to difficulties in the marching procedure, and solutions often could not be obtained.

The gridding scheme of the Rai and Chaussee code was modified to allow ds, the distance from the surface to the first point off the surface divided by the distance from the surface to the shock, to vary in the axial and in the circumferential direction. This was accomplished by the equation

$$ds(i+1,k) = ds(i,k)\,[\text{const}/v(i,k)] \tag{1}$$

Here, i specifies the computational plane, k specifies the radial line, and $v(i,k)$ is the velocity magnitude at the first point off the surface. The constant in the above expression was chosen to be 0.10 times the freestream velocity.

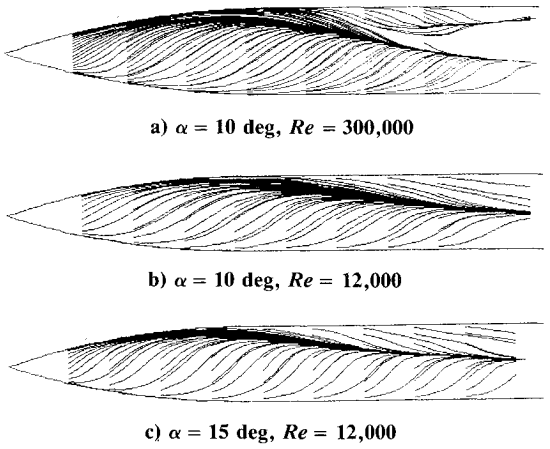

Fig. 2 Side views of the skin-friction patterns.

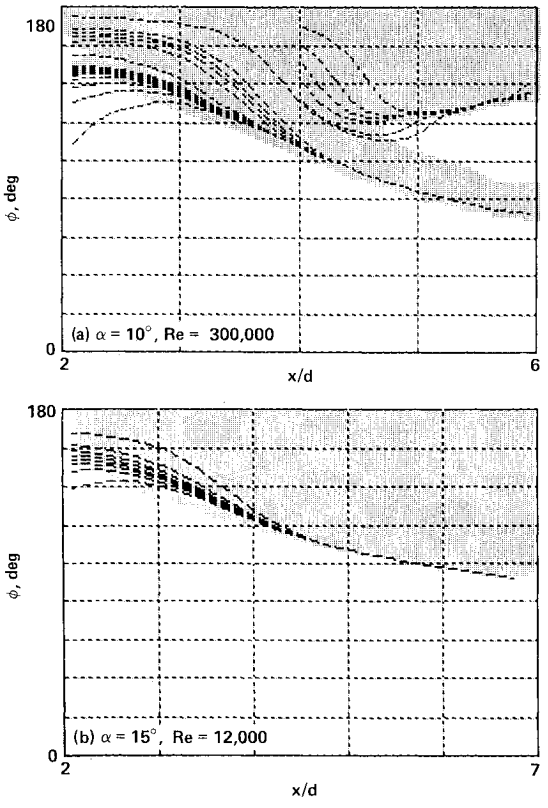

Fig. 3 Skin-friction patterns and regions of negative crossflow. Windward side: ϕ = 0 deg; leeward side: ϕ = 180 deg; distance from the nose: x/d (in calibers).

To maintain a smooth grid in the circumferential direction, $ds(i,k)$ was approximated by a finite Fourier cosine series,

$$ds(i,k) = a_0 + \sum_{m=1}^{3} a_m \cos[m\phi(k)] \tag{2}$$

In the above expression, $\phi(k)$ is the circumferential angle of the kth radial line. Smoothness in the axial direction was accomplished by limiting the amount of change in the a_m by the equations

$$[a_m(i+1) - a_m(i)]/a_m(i) < \delta, \qquad m = 0,1,2,3 \tag{3}$$

$$a_m(i+1)/a_0(i) < \epsilon, \qquad m = 1,2,3 \tag{4}$$

The values of δ and ϵ were chosen to minimize oscillations in the a_m while not affecting the ability of Eq. (2) to adapt the grid; they were generally less than 0.025. With these limitations placed upon the changes in the a_m, the grid changed smoothly and gradually as the solution marched down the body.

Flowfields for three cases ($Re = 300{,}000$, $\alpha = 10$ deg; $Re = 12{,}000$, $\alpha = 10$ deg; and $Re = 12{,}000$, $\alpha = 15$ deg) were computed using a circumferentially clustered grid with a variable ds. Bilateral symmetry was assumed, and the computations were performed for only one side of the cylinder; 73 grid points were used in the circumferential direction, and 45 grid points were used in the radial direction. For the $Re = 300{,}000$, $\alpha = 10$ deg computation, the circumferential spacing of the radial lines at the windward side was 5 deg; at the leeward side this spacing was 3 deg. The minimum spacing was 1.6 deg at 60 deg from the leeward side. For the other two computations, the windward spacing was 5 deg, the leeward spacing was 4 deg; the minimum spacing was 1.4 deg at 80 deg from the leeward side.

To determine if the interpretation of crossflow separation was independent of the gridding, computations of crossflow separation also were performed for grids with uniform spacing in the circumferential direction, for circumferentially clustered grids with fewer points in the boundary layer, and for circumferentially clustered grids with more points in the boundary layer. The number of points in the boundary layer was altered by changing the value of the constant in Eq. (1). These grid modifications did cause small changes in the quantitative values of the pressure and skin friction and in the location of the convergence line but did not effect the qualitative features of crossflow separation.

Results and Discussion

A three-caliber tangent ogive cylinder with a cylindrical diameter of 3.0 in. was used in all computations. The freestream Mach was 2.0, and the freestream temperature was 290°R. The wall temperature was constant at 500°R. Computations were performed for angles of attack of 10 and 15 deg. For $\alpha = 10$ deg, the freestream Reynolds numbers based on body diameter were 12,000 and 300,000. For $\alpha = 15$ deg, the freestream Reynolds number was 12,000. The solutions were marched down the ogive cylinder until crossflow separation and vortex rollup were well established.

The qualitative features of crossflow separation presented in the following sections were found to be independent of both the angle of attack and the Reynolds number, and they can be demonstrated by using only one set of flow conditions. Hence, the discussion of some features of crossflow separation will include the results of only one of the three cases, the $\alpha = 10$ deg, $Re = 300{,}000$ case. The results for all three cases are presented in Yates and Chapman,[7] and a more extensive discussion of crossflow separation can be found in Yates.[8]

Skin-Friction Patterns

Plots of the calculated skin-friction patterns for various angles of attack and Reynolds numbers are shown in Fig. 2. In Figs. 2a and 2b, the skin-friction patterns are shown for a 10 deg angle of attack and Reynolds numbers of 300,000 and 12,000, respectively. In these skin-friction patterns, the convergence line begins closer to the nose for the higher Reynolds number case. In both cases, the circumferential location of the convergence line approaches a constant value as the distance from the nose is increased. For $Re = 300{,}000$, the circumferential location of the convergence line measured from the windward side is approximately 70 deg; for $Re = 12{,}000$, this value is 90 deg. This dependency of the location of the convergence line on the Reynolds number agrees with experimental evidence that indicates that laminar flow separation occurs nearer the nose for higher Reynolds numbers[9] and that, on a yawed cylinder, flow separation occurs more toward the windward side for higher Reynolds numbers.[10] For the $Re = 300{,}000$ computation, a secondary convergence line appears on the leeward side of the primary convergence line. There is no secondary convergence line for the $Re = 12{,}000$ case.

The skin-friction patterns for a constant Reynolds number of 12,000 and two angles of attack, 10 and 15 deg, respectively, are shown in Figs. 2b and 2c. In these patterns, the convergence line begins closer to the nose for $\alpha = 15$ deg than for $\alpha = 10$ deg. This behavior agrees with experimental evidence that indicates that separation occurs nearer to the nose for larger angles of attack.[9] In both cases, the circumferential location of the convergence line approaches a constant value of 90 deg as the distance from the nose increases. Experimental studies at the University of Florida tow tank at subsonic speeds and $Re = 12{,}000$ indicated that for 10 and 15 deg angles of attack the experimental values for the circumferential locations of the convergence lines were near 90 deg.[9]

Crossflow Velocities

In Fig. 3, the regions where negative crossflow velocities occur (flow away from the leeward side) are shown in gray. Also shown are the skin-friction patterns. In these plots, changes from a positive to a negative crossflow velocity occur over a large area on the leeward side within the space of two space-marching steps or 0.067 calibers. These changes are not caused by rapid changes in the flow direction. Before negative crossflow velocities are observed, there is an extended region on the leeward side of the ogive cylinder where the crossflow velocities are small and positive; however, the skin-friction lines are primarily in the axial direction. When negative crossflow velocities are first observed, the skin-friction lines on the leeward side are still primarily in the axial direction.

As soon as a negative crossflow velocity occurs, the velocity fields in the crossflow plane will show what appears to be vortical flow. In Fig. 4a, the crossflow velocity field seems to indicate that separation and vortical flow have occurred at 2.97 calibers aft of the nose for the $\alpha = 15$ deg and $Re = 12{,}000$ computations. This would be an erroneous interpretation. The pseudovortical structures seen in Fig. 4a occur when negative crossflow velocities first appear and the streamlines near the surface begin to squeeze together. However, this squeezing is not at a sufficiently rapid rate for fluid to be forced off the surface and for vortical structures to appear in the fluid. Furthermore, in Fig. 3b there is no evidence of a convergence line at 2.97 calibers aft of the nose. These crossflow velocity fields cannot be used to provide a measure as to when crossflow separation occurs. The appearance of vortical structures in the crossflow plane is a necessary but not sufficient condition for crossflow separation.

Encircling Stream Tubes

A better measure for the onset of crossflow separation than the appearance of vortical structures in the crossflow plane can be obtained by examining crossflow cuts of a stream tube that encircles the body. This stream tube is defined as follows. Initially a circle, $r = r_0$, is defined in the crossflow plane at $x = x_0$ where r is the distance in the crossflow plane from the axis of the ogive cylinder, and x is the axial distance from the nose. The value of x_0 is chosen small enough so that no negative crossflow velocities have occurred and no indications of crossflow separation are observed for $x < x_0$. The stream tube then is defined by the streamlines that pass through each point on this circle. For computational purposes, 360 equally spaced points were used to define the initial circle. Crossflow cuts of these stream tubes that demonstrate the important features of the development of crossflow separation are shown in Fig. 5 for all three cases.

As the limiting streamlines begin to gradually squeeze together, the flow is forced slightly away from the surface, and small bumps occur in the stream tubes, as seen in Figs. 5a and 5c at 2.97 calibers and Fig. 5b at 3.64 calibers. The circum-

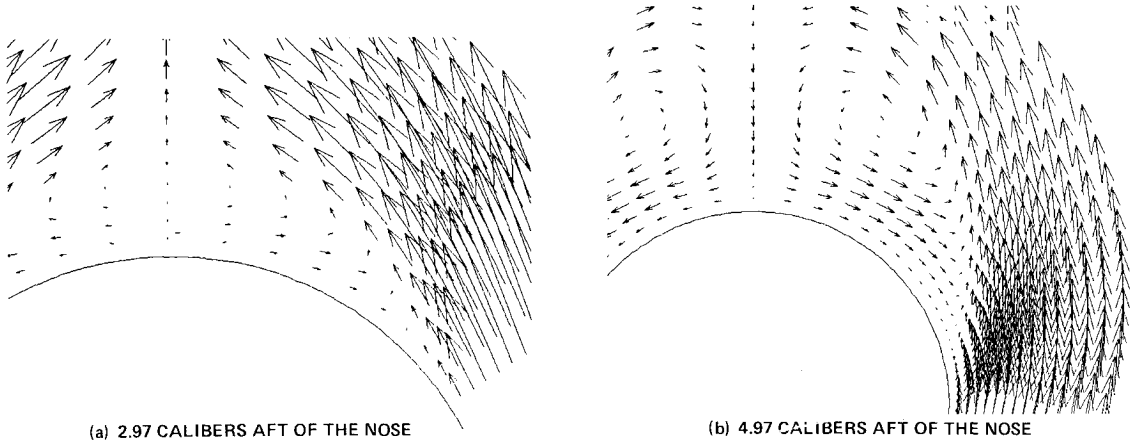

Fig. 4 Crossflow velocities for $\alpha = 15$ deg, $Re = 12{,}000$.

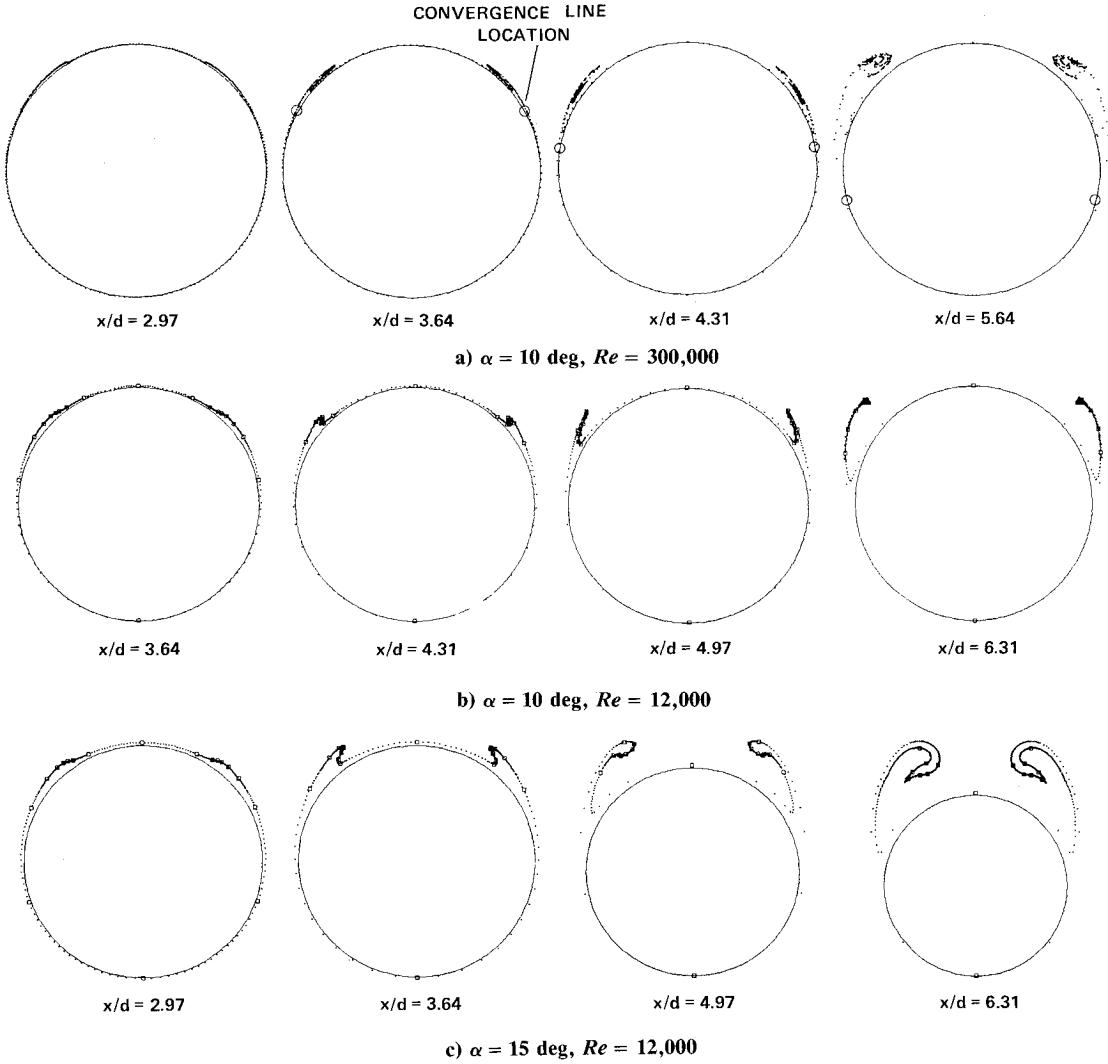

Fig. 5 Crossflow cuts of encircling stream tube.

ferential locations of these bumps coincide with the positions of the converging streamlines. As the distance from the nose increases, the streamlines continue to converge, and the bumps in the stream tubes elongate and fold. For the $\alpha = 15$ deg, $Re = 12{,}000$ case in Fig. 5c, a small fold occurs in the stream tube at 3.64 calibers aft of the nose. In Fig. 3b, the convergence line is not well defined until the distance from the nose is greater than 4 calibers. Hence, these folds in the stream tubes appear before convergence lines can be determined from the skin-friction patterns. The folds continue to elongate and move away from the surface, and the streamlines that define the stream tube and initially were chosen to be uniformly spaced about the body are now clustered onto the folds. The ends of the folds then develop knob-like shapes that coincide with a decrease in Mach number (Fig. 5c, $x/d = 4.97$ calibers), and finally the folds begin to roll up. This behavior of the encircling stream tubes obtained by calculation agrees with the results of the flow-visualization experiments of Intemann.[9]

In Fig. 5, the bases of the folds in the stream tubes widen appreciably near the ogive cylinder's surface. This widening occurred even when the initial circle was chosen to lie between the surface and the first grid points off the surface. Its occurrence indicates that fluid is squeezed off the surface in an extended region and not just in the immediate region of one line, as would be the case if the folds remained narrow all the way to the ogive's surface.

Several values of x_0 and r_0 were tried, and the behavior of the stream tube was not appreciably affected by changes in these variables as long as the stream tube was well within the boundary layer before separation began. The axial location at which a fold first appeared in the stream tube did not change noticeably with changes in x_0 and r_0. Therefore, a reasonable definition of the onset of crossflow separation might be given by the appearance of a fold in the stream tube. This definition implies that crossflow separation begins before a convergence line is observed in the skin-friction pattern but after negative crossflow velocities occur.

Limit Line

Before the convergence line can be determined by visual inspection of the skin-friction patterns in Fig. 2, it is not possible to select one line that becomes the convergence line. It appears that all skin-friction lines are squeezing together to form one line rather than converging on a specific line. After the flow has separated and a convergence line has been established, it appears that the convergence line behaves as an envelope; lines just off the convergence line quickly approach the convergence line and appear to merge with it.

To determine whether the convergence line is indeed an envelope or a limit line, a function $F(n,x)$, which represents the angle that the skin friction makes with respect to the convergence line, was defined as

$$F(n,x) = \left. \frac{\tau_\phi}{\tau_x} - \frac{\tau_\phi}{\tau_x} \right|_{n=0} \qquad (5)$$

In this expression, τ_ϕ is the value of the skin-friction component in the circumferential direction, τ_x is the value of the skin-friction component in the axial direction, x is the axial location of a point on the convergence line, and n is the normal distance from the convergence line. If the convergence line was not well established, $n = 0$ was chosen to be in the center of the bundle of the converging skin-friction lines. In Fig. 6, $F(n,x)$ is plotted for several axial locations on the ogive cylinder for the $\alpha = 10$ deg, $Re = 300{,}000$ case. Initially, the magnitude of the slope $|\partial F/\partial n|$ at $n = 0$ increases as the distance from the nose increases. This indicates that the skin-friction lines approach the convergence line more quickly as the distance from the nose increases.

A maximum value for $|\partial F/\partial n|$ is reached at a finite distance from the nose. This maximum occurs after a fold in the stream tube has occurred, and in two of the cases, $\alpha = 10$ deg, $Re = 300{,}000$ and $\alpha = 15$ deg, $Re = 12{,}000$ (Yates and Chapman,[7] Yates[8]), after the fold has begun to roll up. Once this maximum is reached, $|\partial F/\partial n|_{n=0}$ remains constant or decreases slightly as the distance from the nose is increased. Hence, the slope $|\partial F/\partial n|_{n=0}$ is finite for all axial locations on the ogive cylinder, and the Lipshitz condition is met by the function $F(n,x)$. Therefore, a unique solution exists for the line at $n = 0$, and the convergence line is a limit line, not an envelope.

In Fig. 6, it appears that when a convergence line can be determined from the skin-friction pattern, $n = 0$ is either an inflection point of $F(n,x)$ or is very close to an inflection point. It was not possible to determine whether $n = 0$ was an actual inflection point because of the discrete nature of the data and the linear behavior of the function $F(n,x)$ at $n = 0$.

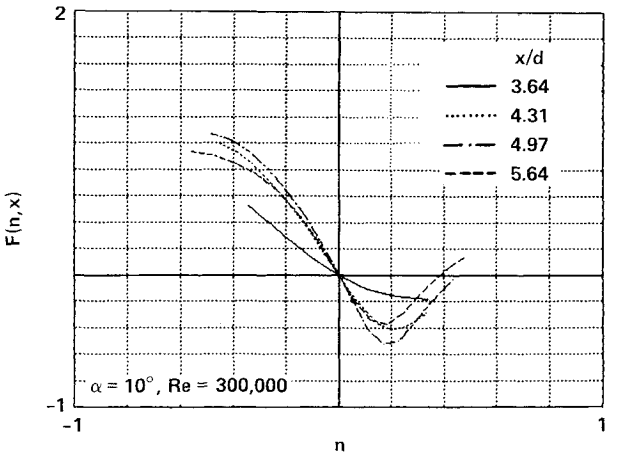

Fig. 6 Angle the skin friction makes with respect to the convergence line.

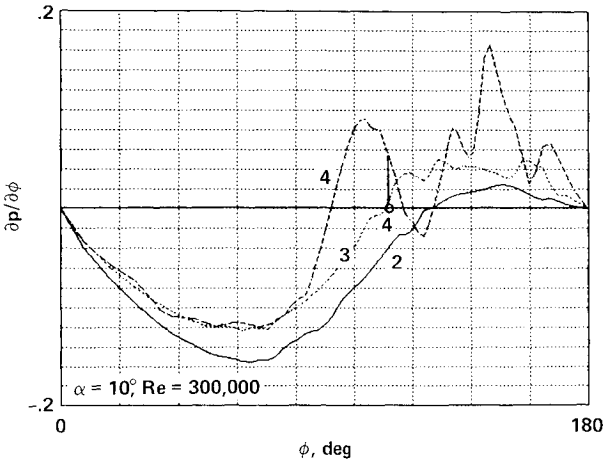

Fig. 7 Circumferential pressure gradients; the numbers represent the distance from the nose in calibers.

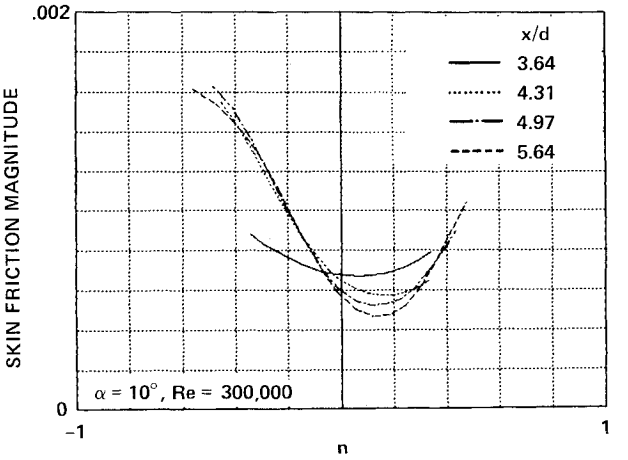

Fig. 8 Skin-friction magnitude.

Flowfield Extrema

Relationships between the location of the convergence line and the locations of extrema in the static pressure, the static pressure gradients, the skin friction, and the angle that the flow made with respect to the surface of the ogive cylinder were also studied. In Fig. 7, the circumferential pressure

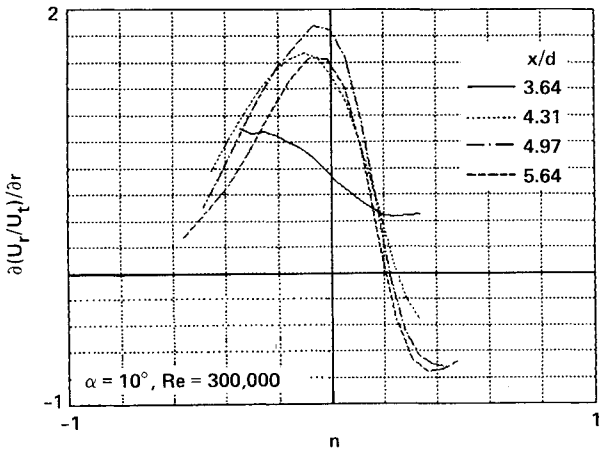

Fig. 9 Flow-angle derivative $\partial/(U_r/U_t)\partial_r$.

gradients $\partial p/\partial\phi$ for the $\alpha = 10$ deg, $Re = 300{,}000$ computation are plotted. There are no abrupt changes in the pressure gradient indicating where separation occurred. There is a pressure gradient maximum on the windward side of the convergence line (in Fig. 7 the location of the convergence line is represented by a circle on the x-axis) and a minimum on the leeward side of the convergence line. Furthermore, since the pressure gradient curve passes through 0 on the windward and leeward side of the convergence line, there is a pressure minimum on the windward side and a pressure maximum on the leeward side of the convergence line. None of the extrema in the pressure and the circumferential pressure gradient coincide with the convergence line.

In Fig. 8, the skin-friction magnitude is plotted against the normal distance from the convergence line. There are no abrupt changes in the behavior of the skin-friction magnitude that indicate where separation occurs. When the convergence line's location can be determined, the minimum in the skin-friction magnitude occurs to the leeward side of the convergence line.

To determine the direction of the flow near the surface of the body, the flow angle U_r/U_t was studied. Here, U_t is the velocity tangent to the surface of the ogive cylinder, and U_r is the velocity normal to the surface. From the continuity equation and the boundary conditions, it can be shown that $U_t = f(x,r,\phi)r$ and $U_r = g(x,r,\phi)r^2$ where x is the axial distance from the nose, r is the normal distance from the surface, ϕ is the circumferential angle, and f and g are functions that are finite at $r = 0$. On the surface the ratio U_r/U_t is equal to 0 unless $f(x,0,\phi) = 0$. This occurs only at a critical point in the skin-friction pattern. Since there are no critical points associated with crossflow separation, $U_r/U_t = 0$ at every point on the surface near the convergence line. At the surface, the first derivative $\partial(U_r/U_t)/\partial r|_{r=0} = g(x,0,\phi)/f(x,0,\phi)$ is not identically zero and is a measure of the flow direction a small distance off the surface. The computed values of $\partial(U_r/U_t)/\partial r$ are plotted against n, the distance measured on the surface along a normal from the convergence line, in Fig. 9. There are no abrupt changes that indicate where separation begins. As the axial distance increases and skin-friction lines squeeze together to form a convergence line, these plots change continuously, and a pronounced peak is formed on the windward side of the convergence line. This peak does not coincide with the convergence line ($n = 0$).

The locations of the maximum pressure gradient, the minimum skin friction, and the maximum flow angle are shown in Fig. 10 for all three cases. These extrema form lines that appear to parallel the convergence line but do not coincide with it. As discussed above, the maximum pressure gradient and maximum flow angle are on the windward side of the convergence line, and the minimum skin-friction line is on the

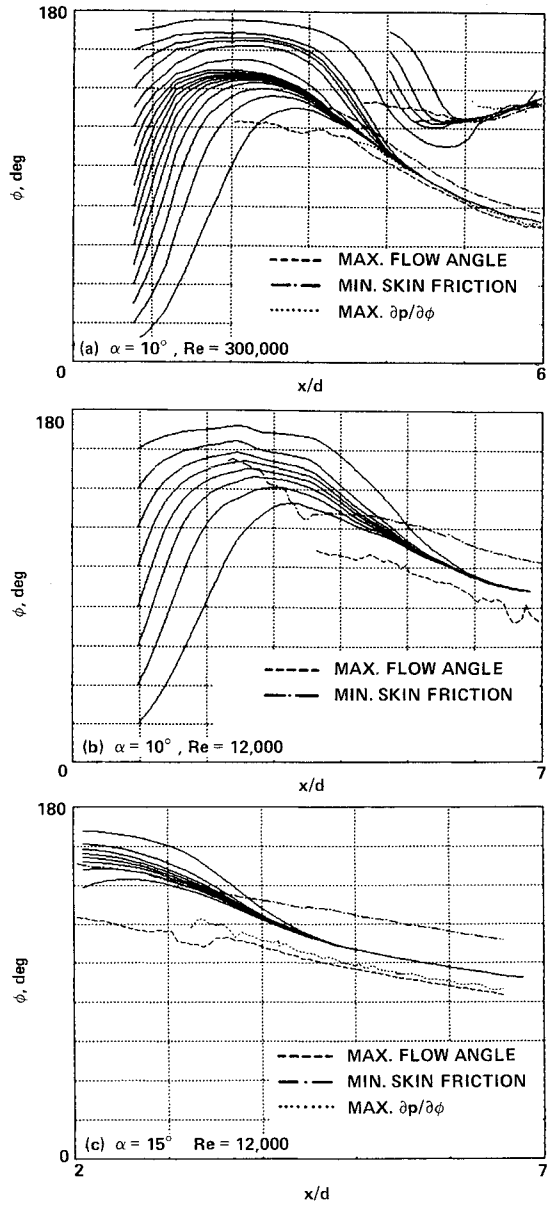

Fig. 10 Skin-friction patterns and circumferential minima and maxima.

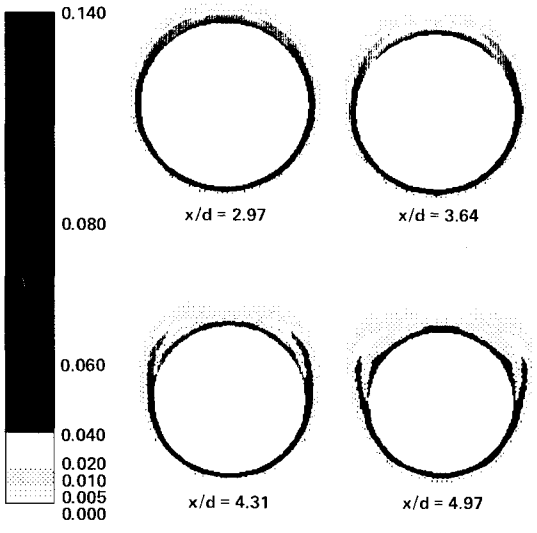

Fig. 11 Vorticity magnitude plotted in crossflow planes, $\alpha = 10$ deg, $Re = 300{,}000$. The vorticity magnitude has been divided by the freestream speed of sound.

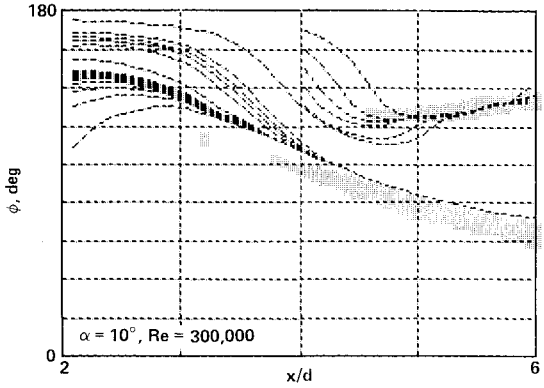

Fig. 12 Regions of $\partial\omega/\partial r > 0$.

leeward side. The offsets of these extrema from the convergence line are sizable for the two $Re = 12{,}000$ cases and are not the result of numerical error. At the higher Reynolds numbers, these offsets diminish drastically and are small even for the secondary line of convergence.

Vorticity Distributions

The minimum in the vorticity magnitude also does not coincide with the convergence line. The viscosity coefficient in the parabolized Navier-Stokes code is calculated by Sutherland's formula and is a function of temperature only. Hence, the viscosity coefficient is constant on the surface, and the vorticity magnitude is proportional to the skin-friction magnitude. Therefore, a minimum in the vorticity magnitude lies to the leeward side of the convergence line.

In Fig. 11, the vorticity magnitude in various crossflow planes is shown for $\alpha = 10$ deg, $Re = 300{,}000$ (in Fig. 11 the radial distance from the surface is multiplied by four to show details of the vorticity distribution). Before there is any evidence of folding in the encircling stream tubes, these plots indicate that in the radial direction there is a vorticity maximum off the surface. This maximum is represented by a change of dark to light to dark as the radial distance is increased and can be seen on the leeward side of the vorticity plot at 2.97 calibers aft of the nose. As the distance from the nose is increased, the existence of this maximum becomes more pronounced until a well-defined vortex sheet can be seen leaving the surface. The position of this vortex sheet generally coincides with a fold in the encircling stream tube.

In Fig. 12, the areas shaded in gray indicate where $\partial\omega/\partial r$ is positive; ω is the vorticity magnitude, and r is the distance normal to the surface. When $\partial\omega/\partial r$ is positive, the vorticity magnitude is increasing as the distance from the surface is increased, and the maximum vorticity must lie off the surface. The regions of positive $\partial\omega/\partial r$ lie to the windward side of the convergence lines and parallel them. The convergence lines are not necessarily included by or adjacent to these shaded areas, although it is these areas that appear to feed the vortex sheets shown in Fig. 11.

Conclusions

The adaptations to the gridding scheme of the parabolized Navier-Stokes code improved the resolution and the stability of the solutions by clustering the points into regions where the skin-friction direction was changing rapidly, by adapting the position of the first point off the surface to the local velocity, and by changing the grid smoothly and gradually as the solution was marched down the body. The flow solutions that were computed by the parabolized Navier-Stokes code for crossflow separation on a tangent ogive cylinder exhibited the correct dependency upon the Reynolds number and the angle of attack.

The parabolized Navier-Stokes computations indicated that crossflow separation on a tangent ogive cylinder is a gradual process. There were no abrupt changes in the pressure, the vorticity, or skin friction that indicated when crossflow separation had occurred. Instead, these variables changed slowly and continuously as the crossflow separation developed.

The absence of abrupt changes in the flow variables made it impossible to determine where crossflow separation actually began unless a technique, such as the encircling stream-tube technique, was employed. The stream tube developed a bump as the skin-friction lines began to converge. This bump became a fold that then elongated and rolled up as the distance from the nose increased. The onset of crossflow separation could be defined by the appearance of a fold in the stream tube.

Folds in the encircling stream tubes occurred after the onset of negative crossflow velocities but before convergence lines could be visually determined from the skin-friction patterns. Before a convergence line was established in the skin-friction pattern, the skin-friction lines appeared to squeeze together to form one line instead of converging on one specific line. Once the convergence line was established in the skin-friction pattern, the skin-friction lines rapidly converged on the convergence line. An investigation of the skin-friction direction near the convergence line showed that the convergence line was a limit line and not an envelope.

The lines of minimum and maximum pressure, the lines of the maximum pressure gradients, the lines of the minimum skin friction, and the lines of the maximum flow angle all paralleled the convergence line. However, none of these lines coincided with the convergence line, and their distances from the convergence line indicated that their offsets from the convergence line were true offsets and not the results of computational errors. The location of the convergence line came nearest to the location of an inflection point in the limiting streamline direction, although it did not precisely coincide with it.

Crossflow separation was fairly well established before a convergence line could be observed in the skin-friction pattern. Therefore, the appearance of the convergence line in the skin-friction pattern and the behavior of the lines defined by extrema in the flow parameters appeared to be consequences of crossflow separation. These properties could be used to indicate that crossflow separation had occurred, but not where crossflow separation began.

Since the maximum flow angle and the convergence line were not coincident, it was not possible to define a circumferential location for crossflow separation. It would be natural to define the separation location as the line at which the flow is leaving the surface at the greatest angle. This definition, however, would not agree with the usual definition of the separation line as the convergence line.

In conclusion, for crossflow separation it may be better to think in terms of a separation region that includes the convergence line rather than a single separation line. This separation region would begin downstream of the onset of negative crossflow velocities but upstream of an observable convergence line. This interpretation would take into account the widening of the stream-tube fold near the surface of the body and the offset from the convergence line of the maximum flow angle. It would also take into account the smooth behavior of the pressure, skin-friction, and flow-angle distributions.

Acknowledgment

Funds for the support of this study have been allocated by the NASA-Ames Research Center, Moffett Field, CA, under Interchange NCA2-42.

References

[1]Tobak, M. and Peake, D. J., "Topology of Two-Dimensional and Three-Dimensional Separated Flows," AIAA Paper 79-1480, July 1979.

[2]Tobak, M. and Peake, D. J., "Three-Dimensional Interactions and Vortical Flows with Emphasis on High Speeds," AGARDograph 252, July 1980.

[3]Wang, K. C., "On the Current Controversy of Unsteady Separation," AIAA Paper 83-0296, Jan. 1983.

[4]Chapman, G. T., "Topological Classification of Flow Separation on Three-Dimensional Bodies," AIAA Paper 86-0485, Jan. 1986.

[5]Schiff, L. B. and Steger, J. L., "Numerical Simulation of Steady Supersonic Viscous Flow," AIAA Paper 79-0130, Jan. 1979.

[6]Rai, M. M. and Chaussee, D. S., "New Implicit Boundary Procedures: Theory and Applications," AIAA Paper 83-0123, Jan. 1983.

[7]Yates, L. A. and Chapman, G. T., "A Numerical Investigation of Crossflow Separation on a Three-Caliber Tangent Ogive-Cylinder," AIAA Paper 87-1209, June 1987.

[8]Yates, L. A., "A Numerical Investigation of Flow Separation on a Three-Caliber Tangent Ogive," Ph.D. Dissertation, Univ. of Florida, Gainesville, FL, 1986.

[9]Intemann, G. A., "Experimental Investigation of the Location and Mechanism of Local Flow Separation on a 3-Caliber Tangent Ogive Cylinder at Moderate Angles of Attack," M.S. Thesis, Univ. of Florida, Gainesville, FL, 1986.

[10]Bursnall, W. J. and Loftin, L. K., Jr., "Experimental Investigation of the Pressure Distribution About a Yawed Circular Cylinder in the Critical Reynolds Number Range," NACA TN 2463, 1951.